Simulation of field injection experiments in heterogeneous unsaturated media using cokriging and artificial neural network

Ming Ye,[1] Raziuddin Khaleel,[2] Marcel G. Schaap,[3,4] and Jianting Zhu[5]

Received 10 March 2006; revised 31 January 2007; accepted 6 March 2007; published 12 July 2007.

[1] Simulations of moisture flow in heterogeneous soils are often hampered by lack of measurements of soil hydraulic parameters, making it necessary to rely on other sources of information. In this paper, we develop a methodology to integrate data that can be easily obtained (for example, initial moisture content, θ_i, bulk density, and soil texture) with data on soil hydraulic properties via cokriging and Artificial Neural Network (ANN)-based pedotransfer functions. The method is applied to generate heterogeneous soil hydraulic parameters at a field injection site in southeastern Washington State. Stratigraphy at the site consists of imperfectly stratified layers with irregular layer boundaries. Cokriging is first used to generate three-dimensional heterogeneous fields of bulk density and soil texture using an extensive data set of field-measured θ_i, which carry signature about site heterogeneity and stratigraphy. Soil texture and bulk density are subsequently input into an ANN-based site-specific pedotransfer function to generate three-dimensional heterogeneous soil hydraulic parameter fields. The stratigraphy at the site is well represented by the estimated pedotransfer variables and soil hydraulic parameters. The parameter estimates are then used to simulate a field injection experiment at the site. A relatively good agreement is obtained between the simulated and observed moisture contents. The spatial distribution pattern of observed moisture content as well as the southeastward moisture movement is captured well in the simulations. In contrast to earlier work using an effective parameter approach (Yeh et al., 2005), we are able to reproduce the observed splitting of the moisture plume in a coarse sand unit that is sandwiched between two fine-textured units. The simple method of combining cokriging and ANN for site characterization provides unbiased prediction of the observed moisture plume and is flexible so that additional measurements of various types can be included as they become available.

Citation: Ye, M., R. Khaleel, M. G. Schaap, and J. Zhu (2007), Simulation of field injection experiments in heterogeneous unsaturated media using cokriging and artificial neural network, *Water Resour. Res.*, *43*, W07413, doi:10.1029/2006WR005030.

1. Introduction

[2] An accurate simulation of moisture flow in heterogeneous vadose zone soils is often difficult because of a lack of site-specific soil hydraulic parameters. Because of limits in measurement techniques, time, and/or budget, measurements of soil hydraulic properties are usually sparse, especially those of moisture retention and unsaturated hydraulic conductivity. By contrast, it is generally easier to obtain data that contain indirect information about spatial structure and heterogeneity of the parameters. Such data may include moisture content, textural, geophysical data, soil-water pressure head, and other quantitative or qualitative information about a site of interest. Various inverse and forward methods have been developed to combine data of multiple types and thereby improve predictions of flow and solute transport in heterogeneous unsaturated media. For example, *Yeh and Zhang* [1996] and *Zhang and Yeh* [1997] developed a cokriging-based geostatistical inverse method to estimate saturated hydraulic conductivity and pore size distribution parameter of the Gardner model [*Gardner*, 1958] using soil-water pressure head and degree of saturation. Later, in modeling three-dimensional unsteady flow, the method was improved by including other data types [*Li and Yeh*, 1999; *Yeh and Liu*, 2000; *Liu and Yeh*, 2004; *Hughson and Yeh*, 2000]. Although inverse modeling can improve estimation of soil hydraulic properties, it is computationally expensive (especially for large-scale problems), because it requires an iterative solution of Richards' equation to improve the estimates.

[3] For many practical applications, various computationally efficient forward methods have been developed to estimate heterogeneous soil hydraulic parameters using a variety of data types. *Rockhold et al.* [1996] developed a method to generate hydraulic properties for flow and transport modeling at the Las Cruces Trench Site using

[1]School of Computational Science and Department of Geological Sciences, Florida State University, Tallahassee, Florida, USA.
[2]Fluor Government Group, Richland, Washington, USA.
[3]Department of Environmental Sciences, University of California, Riverside, California, USA.
[4]Now at Department of Soil Water and Environmental Science, University of Arizona, Tucson, Arizona, USA.
[5]Division of Hydrologic Sciences, Desert Research Institute, Nevada System of Higher Education, Las Vegas, Nevada, USA.

0043-1397/07/2006WR005030$09.00

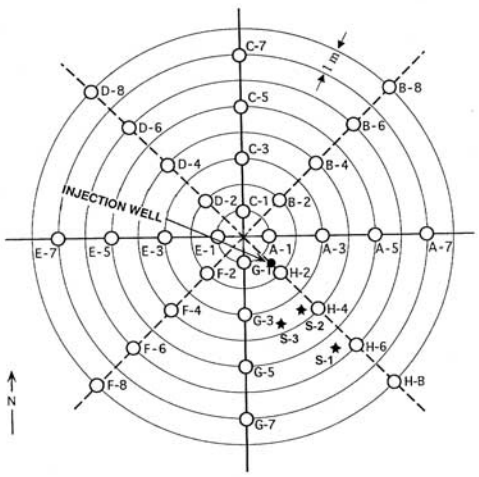

Figure 1. Plan view of the work of *Sisson and Lu* [1984] injection test site and well numbering scheme [after *Gee and Ward*, 2001].

two types of data. One type of data included initial moisture contents and pressure heads measured before the start of a field experiment. The other type of data included the scale-mean (reference) values for hydraulic parameters determined from similar media upscaling. *Meyer et al.* [1997] developed a Bayesian updating method to improve prior probability distributions of soil hydraulic parameters by incorporating sparse on-site parameter estimates. Prior information of soil parameters obtained from literature and similar sites was used as one data type in calculating statistical moments (for example, mean and variance) of parameter distributions. *Wang et al.* [2003] simulated large-scale field infiltration experiments at the Maricopa site near Phoenix, Arizona, using a hierarchy of models based on public, generic, and site data. These data were combined using geostatistical analyses, pedotransfer functions, and Bayesian updating. *Cassiani and Binley* [2005] used borehole geophysical logs to identify soil-layering structure and generated soil hydraulic parameters using prior information about the parameter ranges as constraints. In the preceding studies, in general, a combination of a variety of data types resulted in a better agreement between the observed and simulated variables of interest.

[4] The objective of this study is to develop a new methodology to characterize heterogeneity of soil hydraulic parameters, and simulate an infiltration experiment at the Sisson and Lu (hereinafter referred to as S&L) site (Figure 1) at the U.S. Department of Energy's Hanford Site in Washington State. The new method combines geostatistics and Artificial Neural Network (ANN)-based pedotransfer function (PTF) methods to bridge information from multiple types of data obtained at the S&L site. One type of data is comprised of fitted van Genuchten parameters [*van Genuchten*, 1980] and saturated hydraulic conductivities for 70 core samples [*Khaleel and Freeman*, 1995; *Khaleel et al.*, 1995; *Schaap et al.*, 2003]. These data are, however, insufficient to fully characterize the three-dimensional structure needed for a model to simulate the variably saturated flow at the site. Other types of data include initial moisture content (θ_i) measured at the start of the field injection experiment, bulk density, and soil texture. The extensive database of θ_i carries the signature of media heterogeneity at the site. This is evident from θ_i measurements, which show that larger moisture content (θ) values are representative of fine-textured media, and smaller θ values are representative of coarse-textured media [*Ye et al.*, 2005]. Cross correlations between the initial moisture content, bulk density, and soil texture are first established based on available field data. Cokriging is then used to generate heterogeneous three-dimensional fields of bulk density and soil texture using the measured θ_i field as secondary information. The bulk density and soil texture fields are subsequently input into an ANN-based PTF to generate heterogeneous three-dimensional fields of saturated hydraulic conductivity and van Genuchten model parameters. The ANN is based on laboratory measurements of soil samples obtained at the S&L site [*Khaleel and Freeman*, 1995; *Khaleel et al.*, 1995; *Schaap et al.*, 2003].

[5] The three-dimensional heterogeneous fields of soil hydraulic parameter are used to simulate a field injection experiment conducted by *Gee and Ward* [2001] at the S&L site. The moisture movement at the S&L site, to a large degree, is controlled by media heterogeneity and the imperfectly stratified irregular layer boundaries [*Ye et al.*, 2005]. Therefore an important goal in this study is to explore how well our new method can reproduce, without relying on time-consuming inverse modeling, the imperfectly stratified layers and the three-dimensional structure of the observed moisture plume at the site. The proposed method is viewed as a forward method, since, different from traditional inverse methods, it does not require solving Richards' equation iteratively. Even though our approach requires fitting sample variogram and training ANN, it is computationally more efficient compared to traditional inverse methods.

[6] In this paper, section 2 describes the injection experiment and summarizes previous numerical simulations of the experiment. In section 3, following a discussion of the variety of data used in this study, we present an integration of cokriging and ANN. Results of geostatistical analysis and heterogeneous fields of soil hydraulic parameters generated by ANN are discussed in section 4, which also compares simulated and observed moisture content of the 2000 injection experiment. Conclusions are given in section 5.

2. Description of Field Injection Experiment and Previous Numerical Simulations

2.1. Description of the 2000 Injection Experiment

[7] The S&L injection site (Figure 1) was originally designed by *Sisson and Lu* [1984] within the 200 East Area of the U. S. Department of Energy's Hanford Site in southeastern Washington State. For a description of the S&L site, the reader is referred to the studies of *Ward et al.* [2000], *Gee and Ward* [2001], *Last and Caldwell* [2001], and *Last et al.* [2001]. The S&L site was used for two field infiltration experiments: the first one in 1980 [*Sisson and Lu*, 1984] and the second one in 2000 [*Gee and Ward*, 2001]. In the 2000 experiment, moisture content (θ) distribution was measured at the 32 radially and symmetrically arranged cased boreholes (Figure 1). The initial moisture contents (θ_i), measured on 5 May 2000, reflect soil heterogeneity, especially the imperfectly stratified layered structure at the site [*Ye et al.*, 2005]. Injections began on June 1

and 4,000 liters of water were metered into an injection point 5 m below the land surface over six hours. Similarly, 4,000 liters of water were injected in each subsequent injection on 8, 15, 22, and 28 June. During the injection period, neutron logging in 32 wells took place within a day (i.e., 2, 9, 16, and 23 June) following each of the first four injections. A wildfire burned close to the field site preventing immediate logging of the θ distribution for the fifth injection on 28 June. Three additional readings of the 32 wells were subsequently completed on 7, 17, and 31 July. During each neutron logging, moisture contents were monitored in each well at a depth interval of 0.3048 m (1 ft) starting from a depth of 3.9625 m (13 ft) and continuing to a depth of 16.764 m (55 ft), resulting in a total of 1,376 measurements in each of the eight observation days over a 2-month period. The extensive and dense data set provides a unique opportunity to quantify the dynamics of moisture movement within the vadose zone.

[8] Details on the calibration function for the neutron measurements are given by *Ye et al.* [2005]. To ascertain consistency and accuracy of the neutron readings, the θ_i of the 2000 experiment was plotted against the θ_i of the 1980 experiment; the plot (not shown here) yielded an approximate 1:1 relation, suggesting that the neutron data are consistent and reliable.

2.2. Previous Numerical Simulations at the S&L Site

[9] Several investigators analyzed, with mixed success, the effect of heterogeneity on the 1980 moisture plume using numerical modeling (see summary of *Fayer et al.* [1995] and *Rockhold et al.* [1999]). For the 2000 injection experiment, *Ward et al.* [2000] and *Gee and Ward* [2001] illustrated three-dimensional distribution of θ at the site and evaluated spatial moments of θ up to second order, mean velocity in x, y, and z directions, cumulative travel distance, and path directions. These analyses illustrate the temporal variation of the three-dimensional θ field and the effect of stratigraphy on the movement of injected water. *Zhang et al.* [2004] developed a combined parameter scaling and inverse technique (CPSIT), which uses inverse modeling to resolve the problem of sparse measurements for soil hydraulic parameters. Parameter upscaling was used to shorten computational time. *Ye et al.* [2005] conducted a hierarchical geostatistical analysis of initial moisture content to examine the large-scale geologic structure for the entire site, and investigated small-scale features within different layers. Their variogram analysis shows that the initial moisture content measurements can be viewed as a stationary field. A visualization of the three-dimensional moisture plume evolution illustrated the effect of media heterogeneity, especially the effect of imperfectly stratified layering structure, on moisture movement. Spatial moment analysis was also conducted to quantify the rate and direction of movement of the plume mass center and its spatial spreading. The resulting ratio of horizontal to vertical spreading at varying moisture contents suggested moisture-dependent anisotropy in effective unsaturated hydraulic conductivity, confirming existing stochastic theories [*Yeh et al.*, 1985a, 1985b, 1985c]. However, the principal directions of the spatial moments were found to vary with time as the moisture plume evolved through local heterogeneities, a feature that has not been recognized in theories. Using spatial moments of three-dimensional snapshots of the moisture plume under transient flow conditions, *Yeh et al.* [2005] developed a simple approach to estimate the effective moisture retention and the three-dimensional upscaled unsaturated hydraulic conductivity tensor. The effective parameters reproduced the general behavior of the observed plume at the site. However, because *Yeh et al.* [2005] conceptualized the heterogeneous media as an equivalent homogeneous medium, the simulated ensemble mean behavior did not capture the highly variable, single realization behavior of the observed moisture plume. *Ward et al.* [2006] used a similar upscaling method, and further adjusted upscaled parameters using CPSIT. As discussed in *Yeh et al.* [2005], however, the upscaled unsaturated hydraulic conductivity tensor has its limitations in predicting the detailed behavior of plume dynamics due to the presence of moisture diffusivity lengths that are smaller compared to correlation scales of heterogeneity at the site. A higher resolution model is thus needed to adequately represent media heterogeneity and its effect on plume behavior.

3. Methods

3.1. Description of Multiple Data Sets

[10] Seventy data sets are available based on 70 core samples from six boreholes. Seventeen of them are from boreholes E-7, E-1, and A-7 [*Khaleel and Freeman*, 1995; *Khaleel et al.*, 1995], and 53 from boreholes S-1, S-2, and S-3 [*Schaap et al.*, 2003]. The location of the boreholes is shown in Figure 1, which shows that S-1, S-2, and S-3 are more closely spaced than other boreholes. Each data set contains soil hydraulic properties, including laboratory measurements of saturated hydraulic conductivity (K_s, m/day), saturated moisture content (θ_s, cm^3/cm^3), residual moisture content (θ_r, cm^3/cm^3), and van Genuchten α (1/m) and n (−). The latter four retention variables are obtained by fitting moisture retention data to the van Genuchten model [*van Genuchten*, 1980]

$$S_e(\psi) = \frac{\theta(\psi) - \theta_r}{\theta_s - \theta_r} = \frac{1}{(1 + |\alpha\psi|^n)^{1-1/n}} \quad (1)$$

where S_e is the effective saturation and ψ is the pressure head. Another type of data, called pedotransfer variables in this paper, is included in each data set. It includes bulk density (BD, kg/m^3), gravel content (>2,000 μm) (GR, %), coarse sand content (2,000 to 200 μm) (CS, %), fine sand content (200 to 50 μm) (FS, %), silt content (5 to 50 μm) (SI, %), and clay content (<5 μm) (CL, %). Descriptive statistics of the 70 data sets are listed in Table 1. The dominating particle fractions at the site are coarse and fine sand. The percentage of silt is higher than that of clay, while gravel percentage is the smallest.

3.2. Spatial Structural Analysis and Cokriging

[11] There are 1,376 measurements of initial moisture content (θ_i) in the three-dimensional domain, and they can be used as a surrogate for site heterogeneity. By contrast, the soil hydraulic properties and PTF variables (BD, GR, CS, FS, SI, and CL) are under-sampled (only 70 measurements are available). We first develop three-dimensional heterogeneous fields of the pedotransfer variables (primary variables) using cokriging, with θ_i as the secondary variable. Each of the PTF variables is estimated independently. Since

Table 1. Descriptive Statistics of the 70 Data Sets (Q1, M, and Q3 are Lower Quartile, Median, and Upper Quartile, Respectively)

	Mean	Variance	Min	Q1	M	Q3	Max
BD (kg/m^3)	1575	8877	1394	1513	1580	1634	1870
GR (wt. %)	1.39	7.10	0.00	0.19	0.62	1.53	18.00
CS (wt. %)	76.26	303.34	23.00	70.45	80.79	89.69	97.00
FS (wt. %)	14.93	185.09	1.77	6.57	11.00	18.15	68.00
SI (wt. %)	4.77	25.57	0.00	0.00	3.39	7.78	21.93
CL (wt. %)	2.66	3.90	0.00	1.25	2.50	3.75	7.50
K_s (m/day)	17.68	449.10	0.12	2.89	10.72	25.78	91.22
θ_s (vol. %)	34.74	29.20	21.78	30.65	34.06	38.53	47.42
θ_r (vol. %)	3.09	1.791	0.00	2.357	2.99	3.96	6.719
α (1/m)	9.81	123.46	0.43	3.70	6.70	11.74	62.81
n (−)	2.516	2.674	1.34	1.63	1.913	2.88	11.96

the total number of samples for the PTF variables is the same, estimating them jointly using cokriging is not expected to improve results. The estimated PTF variables are subsequently used as inputs to the ANN (described in section 3.3) to generate heterogeneous soil hydraulic parameters.

[12] Denoting $Z(\mathbf{x}_{Z,0})$ for each of the pedotransfer variables (BD, GR, CS, FS, SI, and CL) at point $\mathbf{x}_{Z,0}$, cokriging $Z(\mathbf{x}_{Z,0})$ is a linear combination of the primary variable and the secondary variable (initial moisture content θ_i denoted as Y) via traditional ordinary cokriging [*Journel and Huijbregts*, 1978]

$$Z^*_{\mathrm{COK}}(\mathbf{x}_{Z,0}) = \sum_{i=1}^{I} u_i(\mathbf{x}_{Z,0}) Z(\mathbf{x}_{Z,i}) + \sum_{j=1}^{J} v_j(\mathbf{x}_{Z,0}) Y(\mathbf{x}_{Y,j}) \qquad (2)$$

where u_i is weight applied to sample Z at location $\mathbf{x}_{Z,i}$ and v_j is weight applied to sample Y at location $\mathbf{x}_{Y,j}$. Cokriging system of equations can be found in the work of *Journel and Huijbregts* [1978], *Yates and Warrick* [1987], and *Isaaks and Srivastava* [1989]. Cokriging entails variograms γ_{ZZ} and γ_{YY} of Z and Y, and cross-variograms γ_{YZ} and γ_{ZY} between Z and Y, which quantify spatial variation and correlation of Z and Y. The variogram and cross-variogram functions can be calculated via [*Journel and Huijbregts*, 1978]

$$\gamma_{ij}(h) = \frac{1}{2N(h)} \sum_{k=1}^{N(h)} [z_i(\mathbf{x}_k) - z_i(\mathbf{x}_k + \mathbf{h})] \cdot [z_j(\mathbf{x}_k) - z_j(\mathbf{x}_k + \mathbf{h})] \qquad (3)$$

where N ($\mathbf{h}$) is the number of sample pairs separated by distance vector $\mathbf{h}$, $z(\mathbf{x}_k)$ is the value of variable z (can be either Z or Y) at location $\mathbf{x}_k$ of the kth data pair, and $z(\mathbf{x}_k + \mathbf{h})$ is the value of the same variable at a separation distance of h of the kth data pair. When $i = j$, γ_{ij} indicates the variogram of variable $z_i = z_j$; when $i \neq j$, γ_{ij} is the cross-variogram of variable z_i and z_j. While a variogram is always positive, a cross-variogram can be negative, indicating that, on average, an increase in one variable corresponds to a decrease in the other variable. All variograms and cross-variograms are expressed using intrinsic coregionalization, a special case of the linear model of coregionalization [*Journel and Huijbregts*, 1978]. An intrinsic coregionalization is justified, since each pedotransfer variable is under-sampled in comparison with θ_i.

[13] The traditional ordinary cokriging of equation (3) may severely limit the influence of the secondary variable $Y(\theta_i)$ on the primary variable Z. A standardized ordinary cokriging can resolve this problem by rewriting equation (3) as

$$Z^*_{COK}(\mathbf{x}_{Z,0}) = \sum_{i=1}^{I} u_i(\mathbf{x}_{Z,0}) Z(\mathbf{x}_{Z,i}) + \sum_{j=1}^{J} v_j(\mathbf{x}_{Z,0}) \left[Y(\mathbf{x}_{Y,j}) - m_Z - m_Y \right] \qquad (4)$$

where m_Z and m_Y are the stationary mean of Z and Y (θ_i). The standardized cokriging is superior to the traditional cokriging, and for an in-depth comparison the reader is referred to *Isaaks and Srivastava* [1989]. Cokriging requires that data be stationary with constant mean and covariance function that depends only on distance between two data points. This requirement is satisfied for the θ_i observations, as discussed in *Ye et al.* [2005]. For the pedotransfer variables, since their measurements are sparse, the stationarity is assumed. The assumption is not unreasonable, since the θ_i field can be used as a surrogate for media heterogeneity. In addition, the correlation of θ_i with pedotransfer variables is strong, as shown in Figure 2 below.

3.3. Artificial Neural Network

[14] Artificial neural network (ANN)-based analysis for estimating soil hydraulic properties has been used by several authors [*Pachepsky et al.*, 1996; *Schaap and Bouten*, 1996; *Minasny et al.*, 1999; *Pachepsky et al.*, 1999]. An advantage of neural networks, compared to traditional pedotransfer functions (PTFs), is that neural networks require no a priori conceptual model. Near-optimal, possibly nonlinear relations that link input data (particle-size data, bulk density, etc.) to output data (soil hydraulic parameters) are obtained and implemented using an iterative calibration procedure. *Schaap et al.* [1998] used neural network analyses to predict van Genuchten moisture retention parameters and saturated hydraulic conductivity. The combination with the bootstrap method [*Efron and Tibshirani*, 1993] provided the confidence intervals for the PTF predictions. For the purposes of this study, we briefly describe some ANN essentials below; for a detailed description of ANN theory the reader is referred to the work of *Haykin* [1994].

3.3.1. Feed-forward Artificial Neural Network

[15] Feed-forward ANNs are most often used to detect patterns in data sets for which no clear underlying physical model exists. A multilayer feed-forward ANN has an input layer (with J nodes corresponding to input variables x_1

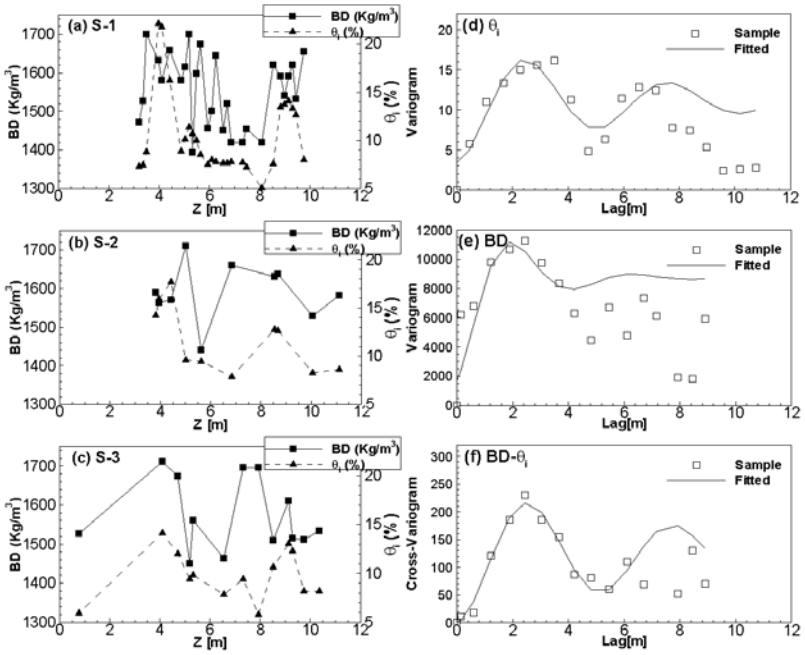

Figure 2. Initial moisture content (θ_i) and bulk density (BD) with elevation at boreholes (a) S-1, (b) S-2, and (c) S-3. Vertical variograms for (d) θ_i and (e) BD and (f) cross-variogram for BD and θ_i.

through x_J), a hidden layer (with K nodes), and an output layer (with L nodes corresponding to output variables y_1 through y_L). The optimal number of "hidden" nodes, K, is problem-dependent and, generally speaking, more hidden nodes allow more complex patterns to be modeled, but also lead to longer optimization times and problems with overparameterization (OP). The mathematical operations inside the network include two matrix-vector multiplications. At each hidden neuron $k = 1$ through K, each input x_j is weighted, summed, and biased (with a value b) to produce a single value, S_k:

$$S_k = \sum_{j=1}^{J} (w_{jk} X_j) + b_k \tag{5}$$

where the coefficients in each layer are positioned in the matrix and vector elements w_{jk} and b_k, respectively. Similar operations occur at the output nodes $l = 1$ through L, with matrices and vectors with elements w_{kl} and b_l, respectively. The values S_k and S_l in hidden and output nodes are transformed by a monotonic "activation" or "transfer" function, φ, that can be easily evaluated [*Hecht-Nielsen*, 1990]. In our case, we use a hyperbolic tangent for the nodes in the hidden layer and a linear function for the nodes in the output layer. The hyperbolic tangent, which produces an output between -1 and 1, is given by

$$\varphi(S_k) = \frac{e^{S_k} - e^{-S_k}}{e^{S_k} + e^{-S_k}}. \tag{6}$$

The linear activation function for the output nodes is simply

$$\varphi(S_l) = S_l. \tag{7}$$

With (7) it becomes possible to generate output values y_1 through y_L outside the range of nonlinear transfer functions, thus avoiding the need to scale output parameters [*Schaap and Bouten*, 1996].

[16] The optimal values for the ANN coefficients (the matrices W_{jk} and W_{kl}, and vectors B_k and B_l) are obtained via the Levenberg-Marquardt algorithm [*Demuth and Beale*, 1992]. The objective function which minimizes the squared residuals over all output variables is

$$O(W_{jk}, B_k, W_{kl}, B_l) = \sum_{n=1}^{N} \sum_{l=1}^{L} (t_{n,l}(W_{jk}, B_k, W_{kl}, B_l) - t'_{n,l})^2 \tag{8}$$

where N is the number of samples, L is the number of parameters (with n and l as index); t and t' are observed and predicted variables (hydraulic parameters), respectively.

3.3.2. Preventing Overparameterization

[17] A frequently occurring problem with ANNs is their tendency to overparameterize if ANN calibration is carried out for too many iterations. Overparameterization (OP) occurs because of the large number of adjustable ANN coefficients that may lock on to noise and data artifacts that are not part of the underlying (and often unknown) physical phenomenon that led to the data set. Typical for overparameterized ANNs is that they perform well for their calibration data sets but that they exhibit degraded performance for independent data. In particular, OP occurs for relatively small data sets such as ours with 70 samples and can be identified by the presence of ANN coefficients with large values [*MacKay*, 1992].

[18] There are two main methods to prevent OP or overtraining. "Early stopping" is a method where the ANN calibration procedure is performed for a limited number of iterations. This can be done by setting a maximum number of iterations that is known to yield an acceptable result, or by evaluating an independent data set during the iterations and force the ANN calibration to stop when the perfor-

mance is optimal on the independent data set [*Schaap et al.*, 1998]. Bayesian regularization [*MacKay*, 1992] is a more graceful method that prevents internal ANN coefficients from becoming too large by including the norm of the coefficients into the objective function:

$$O(W_{jk}, B_k, W_{kl}, B_l) = \alpha \sum_{n=1}^{N} \sum_{l=1}^{L} (t_{nj}(W_{jk}, B_k, W_{kl}, B_l) - t'_{n,l})^2 + (1-\alpha) w^2 \quad (9)$$

where w is the mean of the ANN coefficient matrices (W_{jk} and W_{kl}) and vectors (B_k and B_l), and the parameter α is a problem-dependent weighing factor between 0 and 1, set automatically by the ANN toolbox of MATLAB [*Demuth and Beale*, 1992].

[19] To evaluate the performance of the ANN calibrated with Bayesian regularization, we divided the data set into calibration and independent test sets. To this end, the bootstrap data selection algorithm of *Efron and Tibshirani* [1993] is used to generate 1,000 pairs of calibration and testing data sets out of the original data set of 70 samples. Calibration data sets of size 70 are generated out of the original data set (also of size 70) by random drawing with replacement. Because, on average, only about 63% of the original data is present in each calibration data set (some samples are left out, whereas others are present multiple times), the remaining 37 percent of the samples can be used as an independent test data. An ANN model is calibrated against each calibration data set and tested against the corresponding independent data set. One thousand models are thus calibrated and tested this way and mean errors are computed. For completeness we note that the formal use of the bootstrap method is to generate uncertainty information about estimated parameters [*Efron and Tibshirani*, 1993]. For reasons of brevity, however, such an analysis is not carried out in this study, as it is considered of secondary importance. Here the bootstrap data selection algorithm merely provides a convenient way to generate data sets to compare the performance of ANN-based PTFs on their calibration data and independent test data. Future work may consider the uncertainty in the PTF prediction [*Schaap et al.*, 1998] and evaluate its effects, along with other sources of uncertainty, on simulated flow at the S&L site.

4. Results and Discussions

4.1. Analysis of Spatial Variation and Correlation

[20] Variogram analysis is used to investigate the spatial variation and the correlation between θ_i and the pedotransfer variables (BD, GR, CS, FS, SI, and CL). While horizontal and vertical variograms of θ_i can be calculated [*Ye et al.*, 2005], horizontal variograms (and cross-variograms) of the pedotransfer variables cannot be obtained because their measurements are mainly from boreholes S-1, S-2, and S-3 that are closely spaced in the lateral direction (Figure 1). The variogram analysis is thus limited to the vertical direction. Because of the predominant layered stratigraphy at the S&L site [see *Ye et al.*, 2005, Figure 2], it is not unreasonable to assume that the spatial variation and correlation revealed from the three vertical boreholes are valid over the entire site. Since θ_i at the three boreholes is not available, θ_i values at three neighboring boreholes H-6, H-4, and G-3 (Figure 1) are used. For measurements of the pedotransfer variables at half-foot intervals, the corresponding θ_i is approximated by averaging θ_i above and below the measurements, since θ_i is measured at one-foot interval. For each pedotransfer variable, a total of 53 pairs of θ_i and the primary variable are used for spatial correlation analysis.

[21] The variation in the vertical and the correlation of bulk density (BD) with initial moisture content (θ_i) are first analyzed. Figures 2a–2c illustrate the variation of BD and θ_i with elevation at the three boreholes, respectively. Spatial correlation between the two variables is significant, especially at boreholes S-2 and S-3 (Figure 1). Three sample vertical variograms and cross-variograms of BD and θ_i at the three boreholes are evaluated and then averaged to yield a mean sample vertical variogram and cross-variogram via [*Journel and Huijbregts*, 1978]

$$\gamma_{v,\text{mean}}(h) = \sum_{k=1}^{K} N_k(h)\gamma_{v,k}(h) \Big/ \sum_{k=1}^{K} N_k(h) \quad (10)$$

where $K = 3$ is the number of vertical variograms, $\gamma_{v,k}$, at the three boreholes, and $N_k(h)$ is the number of data pairs corresponding to a vertical lag distance h of the kth elementary variogram. The mean variograms and the cross-variogram are smoother than the elementary ones, and are shown in Figures 2d–2f. The three variograms are of the same shape and exhibit a hole-effect, reflecting periodicity of the fine and coarse material in the stratified media [*Ye et al.*, 2005]. The mean vertical cross-variogram (Figure 2f) shows a positive correlation between BD and θ_i.

[22] Since the sample vertical variograms and the cross-variogram (Figures 2d–2f) are of similar shape, they all are fitted to a dampened hole-effect model [*Deutsch and Journel*, 1998]

$$\gamma(h) = c_0 + c[1.0 - \exp(-3h/d)\cos(h\pi/a)] \quad (11)$$

where c_0 is nugget, c is sill, d is the distance at which 95% of the hole-effect is dampened out, and a is the distance to the first peak and represents the average vertical dimension of layering [*Pyrcz and Deutsch*, 2003]. The variograms are fitted using a generalized least squares method to minimize the objective function [*Cressie*, 1991]

$$\Phi(\mathbf{p}) = \sum_{i=1}^{N} \omega^2 [\gamma^*(h_i) - \gamma(h_i)]^2 \quad (12)$$

where N is the number of lag distances, γ^* is the fitted variogram, ω^2 is the weight for each lag, based on the number of data pairs for the variogram calculation, and $\mathbf{p} = (c_0, c, d, a)$ is the parameter vector. The fitted models are shown in Figures 2d–2f. The value for a is about 2.5 m for the variograms and cross-variogram, suggesting that the average dimension of layered structure at the site is about 2.5 m [*Pyrcz and Deutsch*, 2003], which is again consistent with the finding of *Ye et al.* [2005].

[23] Figure 3 illustrates the sample vertical variograms and cross-variograms for all pedotransfer variables (BD, GR, CS, FS, SI, and CL) and initial moisture content (θ_i). The sample cross-variograms for GR-θ_i and CS-θ_i are

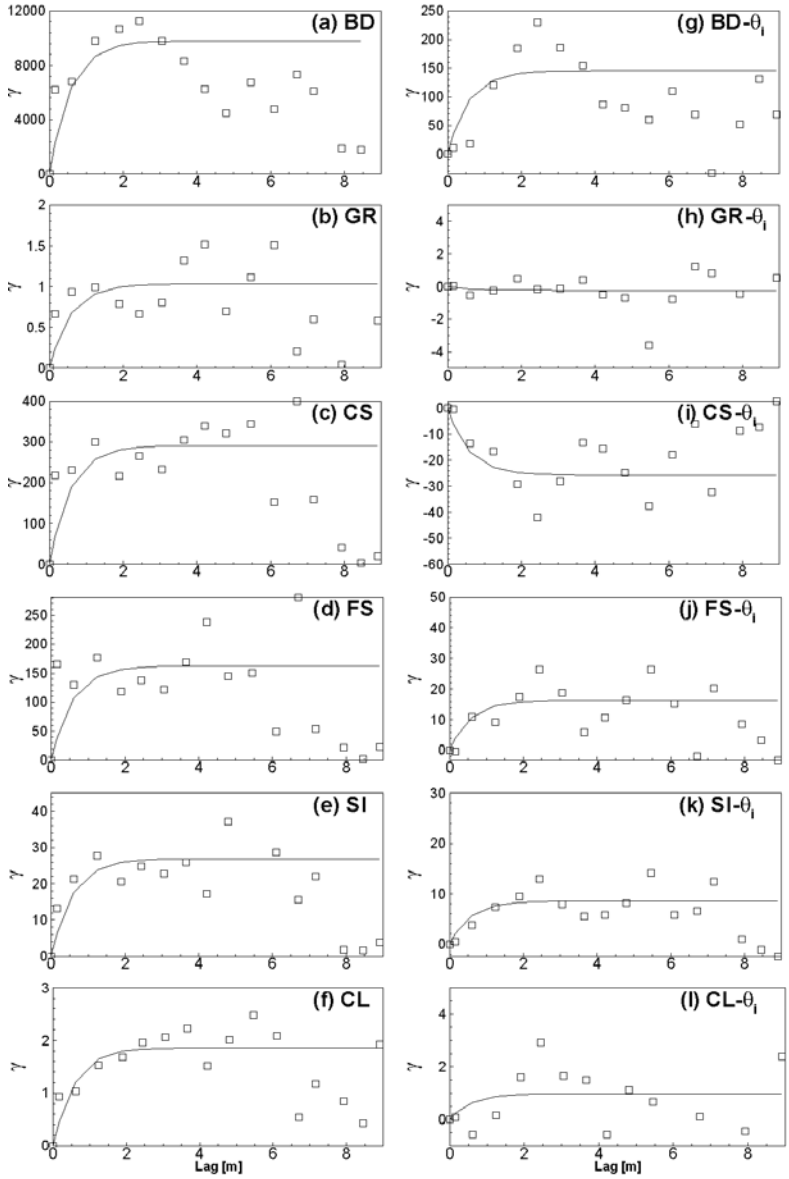

Figure 3. Vertical variograms (a)–(f) for (a) bulk density (BD), (b) gravel (GR), (c) coarse sand (CS), (d) fine sand (FS), (e) silt (SI), (f) clay (CL) percentages and cross-variograms (g)–(l) of the pedotransfer variables and initial water content (θ_i).

negative, indicating that the presence of a coarser fraction (gravel and coarse sand) at the site is negatively correlated with θ_i. Although the hole-effect model appears to be the desired one to fit the sample vertical variograms and cross-variograms, there is no physical reason that such a model is appropriate in the horizontal direction. This is due to the fact that periodicity is not observed in lateral directions, where, instead, extensive continuous layering is present [*Last et al.*, 2001]. Cokriging using hole-effect models fitted from sample vertical variograms gives unreasonable results in the sense that periodicity tends to appear in the lateral directions. Therefore other variogram models (for example, spherical, exponential, and Gaussian) are needed to properly describe spatial variability in both horizontal and vertical directions.

[24] Similar to the work of *Ye et al.* [2005], the sample variogram of θ_i is fitted to an exponential model with geometric anisotropy, which has a sill of 7.36, a horizontal range of 37.76 m, and a vertical range of 1.72 m. Note that the values of the sill and ranges are slightly different from those manually fitted by *Ye et al.* [2005]. Since it is reasonable to use the same variogram model to fit all sample variograms and cross-variograms (see the preceding section), the vertical variograms and cross-variograms in Figure 3 are fitted to the exponential model; the vertical range for initial moisture content is used. Fitted variogram models are shown in Figure 3. Because of the sparse measurements of pedotransfer variables, representative horizontal sample variograms and cross-variograms of the pedotransfer variables and θ_i cannot be calculated. Their horizontal ranges are assumed to be the same as those for θ_i. This assumption is not unreasonable, since the dominant heterogeneity feature at the S&L site is the imperfectly stratified vertical layering structure. This assumption results

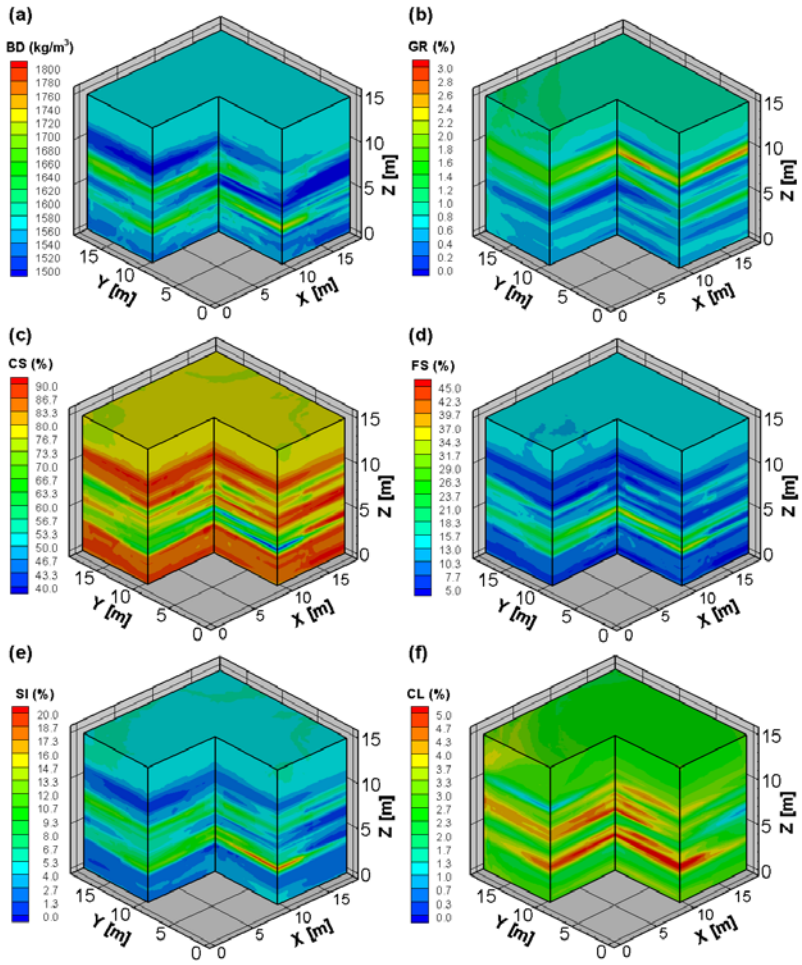

Figure 4. Three-dimensional cokriged heterogeneous fields of pedotransfer variables: (a) bulk density (BD) and percentages of (b) gravel (GR), (c) coarse sand (CS), (d) fine sand (FS), (e) silt (SI), and (f) clay (CL).

in an intrinsic coregionalization of variogram models. It is worth mentioning that fitting the variograms in Figure 3 using hole-effect models yields a better fit. However, as mentioned before, using the fitted hole-effect model for cokriging gives unreasonable results with periodicity in the lateral direction.

4.2. Cokriging to Generate Heterogeneous Fields of Pedotransfer Variables

[25] Using the 1,376 measurements of θ_i as the secondary variable, cokriging is performed using the numerical routine COKB3D of GSLIB [*Deutsch and Journel*, 1998]. Heterogeneous fields for the pedotransfer variables (BD, GR, CS, FS, SI, and CL) are generated. Values of m_Z and m_Y in equation (4) are assigned as means of the pedotransfer variables listed in Table 1, assuming that they are unbiased. Mean initial moisture content is 8.46% for all θ_i measurements. Because cokriging is independently conducted for each of the pedotransfer variables, there is no guarantee that, for each cokriging block, the actual sum of soil texture percentages would be 100%. In our results, for all cokriging blocks, the minimum and maximum difference between the actual sum and 100% is −12% and 14%, respectively, and the mean difference is 2%. This indicates that the cokriging results are reasonable. The soil texture percentages are normalized by the sum of cokriged percentages, and the resulting three-dimensional fields are shown in Figure 4. The effect of imperfectly stratified layering structure is clearly noticeable, and is similar to that of θ_i. Figure 5 compares the spatial variability of measured pedotransfer variables at borehole location S-1 (Figure 1) and the cokriged variables at the nearest cokriging point (0.18 m away from S-1). Note that the vertical intervals of the cokriging values are also different from those of measurements. It is evident from Figure 5 that some of the extreme values are not captured well by the cokriging. This is not surprising due to the well-known smoothing effect of (co)kriging. It is also possible that some thin lenses of fine sediments and other small-scale heterogeneities are not adequately represented by cokriging. Nonetheless, the bulk of the measurements are represented well, indicating that cokriging is a viable approach to represent the S&L site heterogeneity using θ_i measurements as secondary information.

4.3. Development of ANN Pedotransfer Functions

[26] Two types of ANN models are developed. The first one uses all available input variables (BD, GR, CS, FS, SI,

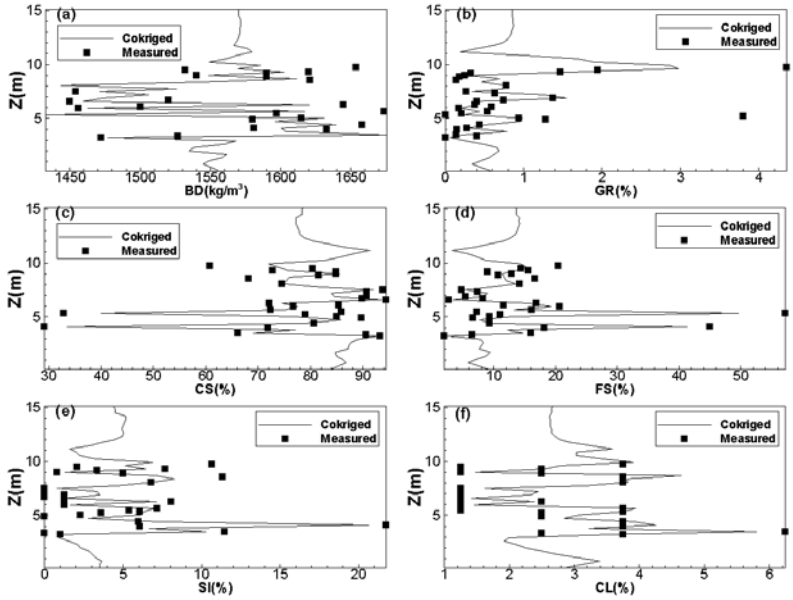

Figure 5. Comparison of cokriged (solid line) and measured (square) pedotransfer parameters at borehole S-1 (location shown in Figure 1).

and CL) to predict θ_r, θ_s, log(α), log(n), and log(K_s), whereas the second one conducts principal component analysis on the input data and uses transformed data from the three, two, or single most important principal components (referred to as PC3, PC2, and PC1, respectively). Both methods are evaluated for six ANN topologies with one to six hidden nodes. As discussed in section 3.3, the performance of each ANN is evaluated for both independent calibration and testing data. Mean root mean square errors are calculated for the retention characteristic and the logarithm of saturated hydraulic conductivity data for all samples in the calibration and testing data sets. For moisture retention, root mean square errors $\mathrm{RMSE_R}$ ($\mathrm{cm^3/cm^3}$) for a calibration or testing data set of N samples retention characteristic is

$$\mathrm{RMSE_R} = \frac{1}{N}\sum_{i=1}^{N}\sqrt{\frac{1}{M_i-4}\sum_{j=1}^{M_i}[\theta'(\mathbf{P}_i,\psi_j)-\theta_j]^2} \qquad (13)$$

where M_i is the number of retention points in the ith characteristic, θ' is calculated moisture content given estimated van Genuchten parameter $\mathbf{P}_i$ (i.e., θ_r, θ_s, α, and n) at pressure head ψ_j, and θ_j is the observed moisture content at pressure head ψ_j. Likewise, the $\mathrm{RMSE_K}$ (without units due to log transformed K_s) for log(K_s) is

$$\mathrm{RMSE_K} = \sqrt{\frac{1}{N}\sum_{i=1}^{N}[\log(K_s')-\log(K_s)]^2} \qquad (14)$$

where K_s' and K_s are estimated and measured saturated conductivity values, respectively.

[27] The neural network results are listed in Table 2. First, the results show that the root mean square errors (RMSE) for calibration data set are always lower than those for the validation data set. This may indicate that the ANNs are still somewhat overparameterized. Similar results were found in the work of *Schaap et al.* [1998]. It should be noted, however, that the calibration and validation results for the PC1 models are relatively close. Second, the RMSEs are relatively low: probably a result of use of a uniform data set from a single site. The RMSE in Rosetta [*Schaap et al.*, 2001] was about 0.068 $\mathrm{cm^3/cm^3}$ for a large heterogeneous data set, whereas validation errors in this study are as low as 0.039 $\mathrm{cm^3/cm^3}$, indicating a better performance. Third, it appears that the ANN results based on the one to three principal components (PC1 through PC3) are somewhat better (by 5 to 10%) than the model that uses all six untransformed input variables.

[28] The optimum validation results for the retention characteristic are reached for PC2 with four hidden nodes, even though several other PC2 and PC1 models have $\mathrm{RMSE_R}$ values that are close to 0.039 $\mathrm{cm^3/cm^3}$ (the minimum); standard errors for each of these models are approximately 0.0005 $\mathrm{cm^3/cm^3}$ (data not shown). The optimum model for K_s is PC2, with two hidden nodes ($\mathrm{RMSE_K}$ is 0.4722); PC3, with one hidden node, is a close second. Standard errors are generally on the order of 0.01 (results not shown). It therefore appears that no model can be identified that has an optimal performance for both retention parameters and K_s. A good compromise is PC2, with three hidden nodes, which is used to generate heterogeneous soil hydraulic parameter fields described below.

4.4. ANN to Generate Heterogeneous Soil Hydraulic Parameter Fields

[29] Using heterogeneous pedotransfer variables generated by cokriging, the ANN-PTF is employed to generate heterogeneous fields of the soil hydraulic parameters: saturated hydraulic conductivity, K_s, and the van Genuchten water retention parameters. Figure 6 illustrates the three-dimensional parameter fields for the soil hydraulic parameters (the residual moisture content is not included for convenience of presentation). Figure 6 again exhibits the imperfectly stratified layering structure present at the S&L site. Similar to Figure 5, Figure 7 compares spatial

Table 2. Artificial Neural Network Calibration (Cal) and Validation Errors (Val) for Four Models With One to Six Hidden Nodes[a]

Hidden Nodes	1	2	3	4	5	6	
Untransformed							
VG-cal	0.0434	0.0387	0.0353	0.0348	0.034	0.0333	cm^3/cm^3
VG-val	0.0461	0.0436	0.0419	0.0427	0.0444	0.0449	cm^3/cm^3
Ks-cal	0.386	0.339	0.316	0.261	0.253	0.233	–
Ks-val	0.521	0.536	0.553	0.581	0.599	0.620	–
Transformed (PC1)							
VG-cal	0.0414	0.0386	0.0379	0.0374	0.0375	0.0366	cm^3/cm^3
VG-val	0.0432	0.0417	0.0412	0.0394	0.0397	0.0394	cm^3/cm^3
Ks-cal	0.469	0.467	0.468	0.457	0.461	0.447	–
Ks-val	0.499	0.504	0.495	0.506	0.509	0.528	–
Transformed (PC2)							
VG-cal	0.0415	0.0383	0.0357	0.0328	0.0325	0.0322	cm^3/cm^3
VG-val	0.0439	0.041	0.0398	0.0390	0.0394	0.0396	cm^3/cm^3
Ks-cal	0.415	0.413	0.388	0.368	0.376	0.372	–
Ks-val	0.494	0.472	0.504	0.548	0.525	0.536	–
Transformed (PC3)							
VG-cal	0.0422	0.0382	0.036	0.0339	0.0325	0.0327	cm^3/cm^3
VG-val	0.0448	0.0419	0.0406	0.040	0.0411	0.0417	cm^3/cm^3
Ks-cal	0.417	0.401	0.364	0.347	0.340	0.334	–
Ks-val	0.477	0.504	0.521	0.551	0.558	0.594	–

[a]"Untransformed" refers to models where all six input variables are input to the ANNs. PC1, PC2, and PC3 are the cases where transformed one, two, or three principal component variables were input to the ANNs.

variability of the measured and ANN-generated soil hydraulic parameters at borehole location S-1 (Figure 1). Although mean values of the ANN estimates agree well with those based on measurements (data not shown), the figure shows that spatial variability of ANN-generated parameters is smaller. This may be due to three reasons. First, the inputs of the ANN, the cokriging results, are smooth, and, as shown in Figure 5, some extreme values are not captured. Second, measurement and fitting errors for soil hydraulic parameters are not accounted for by the derived ANN model. For example, Table 1 shows that the upper quartiles for all parameters are significantly smaller than their maximums. And finally, the ANN models have limitations in their performance as indicated by the RMSE values. This suggests that the six pedotransfer variables (BD, GR, CS, FS, SI, and CL) may not convey all the information needed to estimate the soil hydraulic parameters, which essentially leads to limited output ranges.

4.5. Numerical Simulation of the 2000 Injection Experiment

[30] The generated soil hydraulic parameters are used to simulate the 2000 injection experiment at the S&L site. Simulated and observed moisture contents are compared to evaluate accuracy and robustness of our methodology in characterizing heterogeneous soil hydraulic parameters. The planar area of the simulation domain is 18 × 18 m to include the entire sampling area depicted in Figure 1.

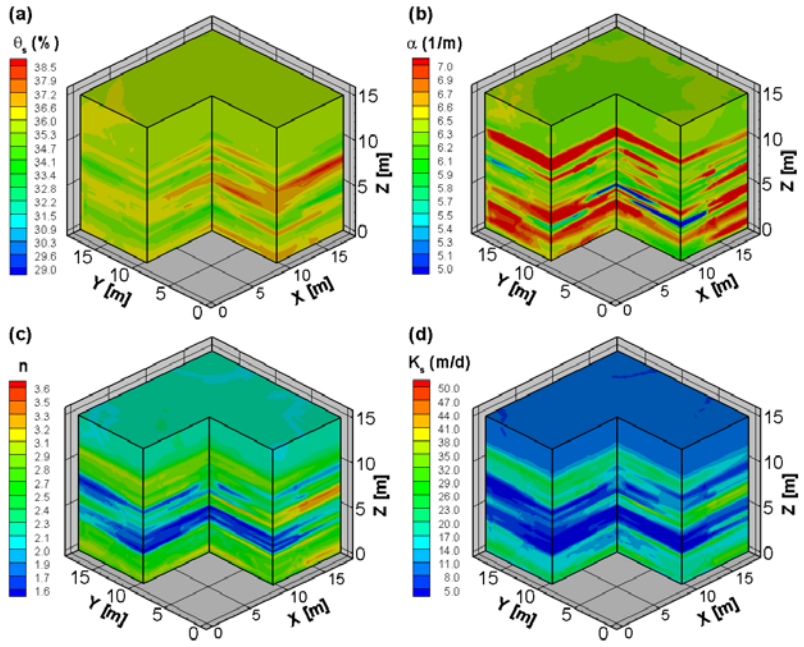

Figure 6. Three-dimensional soil hydraulic parameter fields for (a) saturated water content (θ_s), (b) van Genuchten α, (c) van Genuchten n, and (d) saturated hydraulic conductivity (K_s).

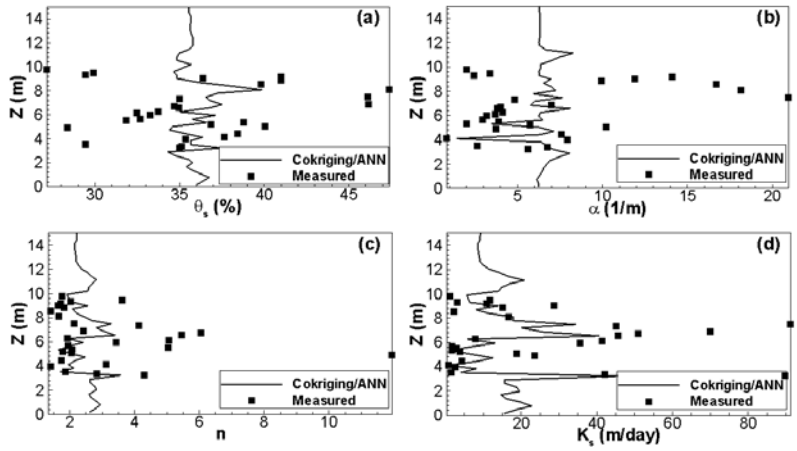

Figure 7. Comparison of ANN-generated (solid line) and estimated (square) (a) saturated water content (θ_s), (b) van Genuchten α, (c) van Genuchten n, and (d) saturated hydraulic conductivity (K_s) based on borehole S-1 samples.

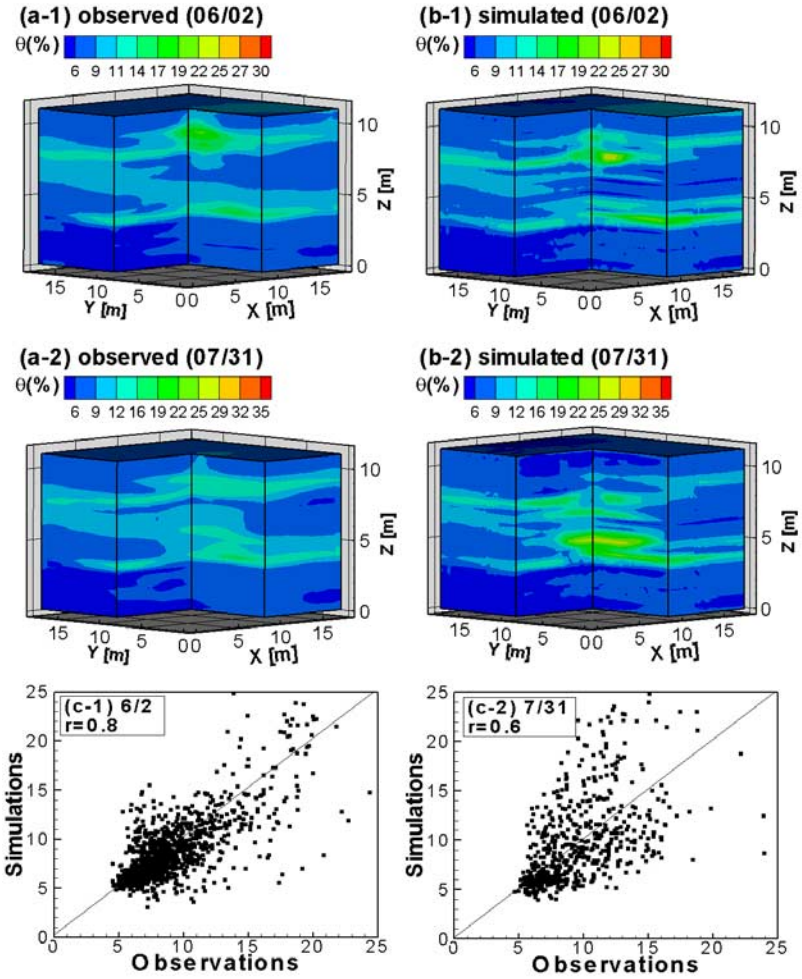

Figure 8. (a-1 and b-1) Three-dimensional fields of observed (a-1) and simulated (b-1) water content on 2 June 2000; (a-2 and b-2) three-dimensional fields of observed (a-2) and simulated (b-2) water content on 31 July 2000. (c-1 and c-2) simulated and observed water content on 6/2 and 7/31. Pearson's linear correlation coefficients (r) are calculated for the two simulation times.

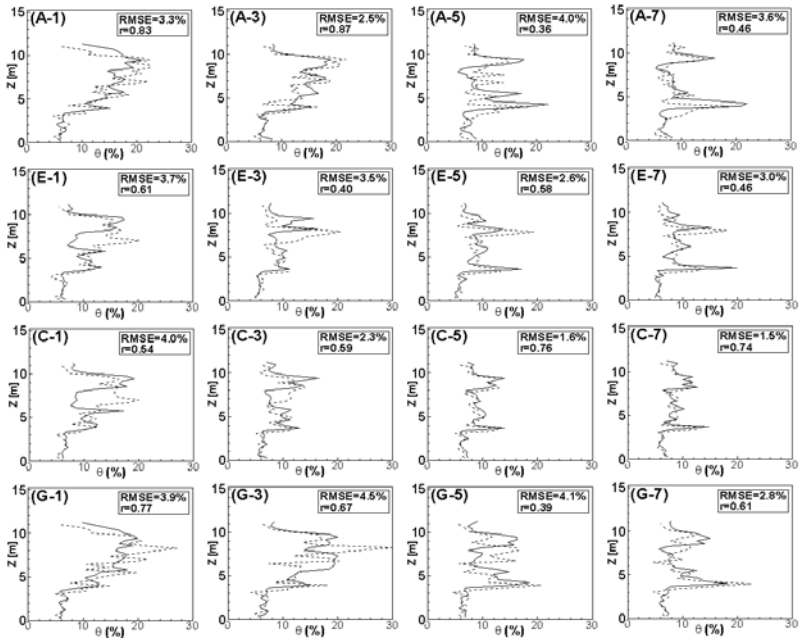

Figure 9. Comparison of simulated (dashed) and observed (solid) moisture content on 23 June 2000 at 16 boreholes, where water contents are directly simulated at grid nodes. Root-mean square-error (RMSE) and Pearson's linear correlation coefficients (r) are calculated for each borehole.

Although moisture contents were measured to a depth of 16.775 m, the vertical dimension of the simulation domain is 15.24 m. This is due to the fact that movement of the injected water is hindered by the second layer of fine-material, and the moisture content below the depth of 15 m essentially remains unchanged in the 2000 injection experiment [*Ye et al.*, 2005]. In other words, location of the domain bottom has negligible effect on simulation results, as long as it is several meters away from the second layer of fine material. This is confirmed by our simulated vertical flux, which is nearly zero at the domain bottom. The simulation domain is discretized into a grid with 259,200 uniform elements, each of which is of 0.25 m (Δx) $\times$ 0.25 m (Δy) $\times$ 0.3048 m (Δz). Such a discretization ensures that the moisture contents for the 16 orthogonally aligned borehole sites starting with A, C, E, and G (Figure 1) are simulated directly. The same grid is also used in generating the heterogeneous pedotransfer variables by cokriging and the soil hydraulic parameters by ANN.

[31] The 2000 injection experiment is simulated using the MMOC code [*Srivastava and Yeh*, 1992], which was also used in our earlier work [*Yeh et al.*, 2005]. The pre-injection tensiometer measurements are not available at the S&L site. The initial pressure head needed for the simulation is therefore based on equation (1), wherein θ_i is estimated using kriging and the ANN-derived soil hydraulic parameters described in section 4.4. Constant head boundary conditions are assumed for all sides of the simulation domain with pressure head equal to the estimated initial head. A prescribed head boundary condition for lateral boundaries is preferred over a no-flow boundary condition, because the simulation results near the boundaries are impacted by the time the injected water starts to leave the flow domain. The constant head boundary allows the injected water exiting the simulation domain, and is thus more realistic than the no-flow boundary. The anisotropy (K_h / K_v) for the local-scale horizontal (K_h) to vertical (K_v) saturated hydraulic conductivity at the site is unknown, and a range between 2 and 60 has been used by other researchers [*Sisson and Lu*, 1984; *Pace et al.*, 2003; *Zhang et al.*, 2004; *Ward et al.*, 2006; *Mayes et al.*, 2003]. A value of 10 is used in our simulations, based on the Hanford Site inverse groundwater modeling [*Cole et al.*, 2001].

[32] Figure 8 compares observed (Figures 8a-1 and 8b-1) and simulated (Figures 8a-2 and 8b-2) moisture content on 2 June 2000 (the first observation date) and 31 July 2000 (the last observation date). Note that no θ measurements were made above an elevation of 11.275 m. Results at other observation times are similar and are not shown. Figure 8 shows that the overall shape and local variation of the observed moisture plumes are simulated well. The goodness of fit is also measured by Pearson's linear correlation coefficients (r = 0.8 for 6/2 and 0.6 for 7/31) between the simulated and observed moisture contents (Figures 8c-1–8c-2). Furthermore, the effect of imperfectly stratified layering structure on moisture movement is captured well, as shown in Figure 8. The injected water spreads in the top layer of fine material at an elevation of about 9 m. The vertical movement of the injected water is retarded by the bottom layer of fine material at an elevation of about 5 m. Between these two layers of fine materials is a layer of coarse material, where the plume splits. Such a separation of the plume beneath the top layer of fine material is well represented in the simulation. Such a separation is also achieved by *Kowalsky et al.* [2005] using inverse modeling in conjunction with use of both neutron probe and cross borehole radar data. In their study, inverse modeling using only neutron data did not result in the plume separation. However, our method yields a similar plume separation with incorporation of only the neutron data. In addition, our forward method does not require solving the Richards' equation iteratively, and is more computationally efficient than traditional inverse methods. It

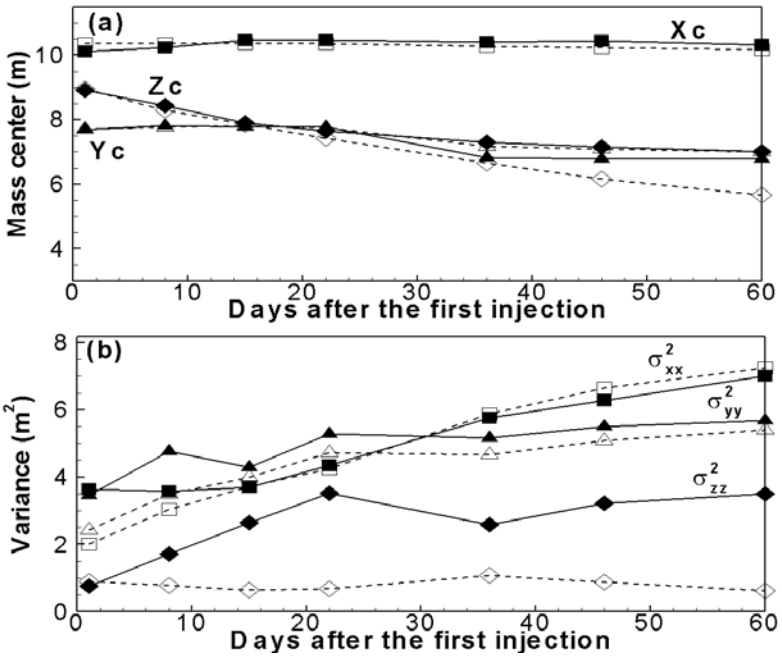

Figure 10. Comparison of observed (filled symbol and solid line) and simulated (open symbol and dashed line) (a) first and (b) second moment of moisture plume.

is worth noting that in our earlier work [*Yeh et al.*, 2005], we conceptualized the heterogeneous media at the S&L site as an equivalent homogeneous medium. Thus we essentially simulated the ensemble mean behavior and, unlike results shown in Figure 8, did not capture the highly variable, single realization behavior of the observed moisture plume and its splitting within the coarse-textured layer that is sandwiched between two fine-textured layers [see *Yeh et al.*, 2005, Figure 9]. Note that a 5-layered model, based on measured data on core samples, was also considered (results not shown here). Compared to the observed plume and unlike results shown in Figure 8, the layered model plume was regular and resulted in a much more uniform spread of the injected water, because each layer was assumed to be homogeneous. Also, unlike results shown in Figure 8, the layered model simulations resulted in a rather mild splitting of the plume.

[33] Besides the results shown in Figure 8 which include the smoothing effect of contouring [*Isaaks and Srivastava*, 1989], the spatial variability of simulated θ is examined at each borehole. Figure 9 compares the observed and simulated θ on 23 June 2000 (the last measurement date following injections) at each of the 16 borehole sites starting with A, C, E, and G (Figure 1). Since the boreholes are aligned horizontally and vertically with the simulation nodes, the θ values are simulated directly at these boreholes. Similar results (not presented here) were obtained for the other 16 boreholes at other observation times. Root-mean square-error (RMSE) and Pearson's linear correlation coefficient (r) values are calculated for each borehole site, and presented in Figure 9. These statistics indicate that the simulated and observed moisture contents agree reasonably well. The RMSE ranges from 1.49 to 4.56% with an average of 3.18%, which are comparable with those obtained through inverse modeling (for example, 2.59% of *Zhang et al.* [2004] and 1.87% of *Ward et al.* [2006]). The r values range from 0.36 to 0.87 with an average of 0.60, indicating that the overall moisture content variation in the vertical direction is captured reasonably well.

[34] Spatial moments (up to the second order) of the simulated as well as the observed moisture difference are calculated in a manner similar to that of *Ye et al.* [2005]. Denoting $\theta_{\text{diff}} = \theta - \theta_{\text{i}}$ as the moisture content difference between moisture content at an observation time and the initial moisture content, we report the spatial moments of θ differences [*Aris*, 1956]

$$M_{ijk}(t) = \int_{-\infty}^{+\infty}\int_{-\infty}^{+\infty}\int_{-\infty}^{+\infty} \theta_{\text{diff}}(x,y,z,t)x^i y^j z^k \mathrm{d}x\mathrm{d}y\mathrm{d}z. \quad (15)$$

[35] The zeroth, first, and second spatial moments correspond to $i + j + k = 0$, 1, and 2, respectively. The zeroth moment (M_{000}) represents the changes in moisture storage within the domain. The normalized first moments,

$$X_{\text{c}} = M_{100}/M_{000} \quad Y_{\text{c}} = M_{010}/M_{000} \quad Z_{\text{c}} = M_{001}/M_{000} \quad (16)$$

represent the location (X_{c}, Y_{c}, Z_{c}) of the mass center of the plume at a given time. The spread of the plume about its center in principal directions is

$$\sigma^2_{xx} = \frac{M_{200}}{M_{000}} - X_{\text{c}}^2 \quad \sigma^2_{yy} = \frac{M_{020}}{M_{000}} - Y_{\text{c}}^2 \quad \sigma^2_{zz} = \frac{M_{002}}{M_{000}} - Z_{\text{c}}^2 \quad (17)$$

The mean moisture plume and its spreading can provide more insights than Figures 8 and 9 into the overall shape of the simulated moisture plume.

[36] Figure 10 shows the plume center [equation (16)] and its spatial variance [equation (17)] for simulated and observed moisture contents at seven different times. The calculated moments for the observed moisture plume are slightly different from those of *Ye et al.* [2005], because the coordinate system is changed and new variogram para-

meters are used based on the automated variogram fitting method. While the simulated X_c and Y_c agree well with the observed values, the simulated Z_c is smaller than the observed Z_c during the redistribution period after injections ceased on 28 June 2000. Compared to the observed data, this indicates a faster downward movement of the simulated moisture plume. For the second moment, while the simulated σ^2_{xx} and σ^2_{yy} agree well with the measured values, the simulated σ^2_{zz} is smaller than the observed value. This indicates a smaller spreading in the z direction for the simulated plume, compared to the observed plume. With the simulated Z_c smaller than the observed Z_c, the simulated moisture movement is faster than that observed in the vertical direction, and less moisture is retained within the profile during downward movement. At the S&L site, fine over coarse sequences produce a series of natural capillary breaks that could impede vertical flow and promote lateral flow within the fine textured layers until the water entry pressure of the coarser soils is exceeded. As the injection progressed, water penetrated the upper coarse layer and started to spread above and in the deeper fine-textured layer. It is possible that the alternate fine and coarse-textured layering is not captured optimally by the cokriging and ANN based on the available data. It is also possible that sediment layers thinner than the simulation grid scale had an additional effect on the vertical infiltration process. Such layers were occasionally observed in the field [*Last and Caldwell*, 2001; *Schaap et al.*, 2003], but could not be adequately sampled.

5. Conclusions and Future Research

[37] Using cokriging and Artificial Neural Network (ANN), we develop a new method to generate heterogeneous soil hydraulic parameters based on a variety of data. The method is applied at the S&L site of the U.S. Department of Energy's Hanford Site. The hydraulic parameters generated are used to simulate the 2000 field injection experiment within the imperfectly stratified media at the S&L site. The soil hydraulic properties data include laboratory measurements of saturated hydraulic conductivity and van Genuchten moisture retention parameters obtained from 70 core samples. Another type of data used, also referred to as pedotransfer (PTF) variables, are bulk density (BD) and percentages of gravel (GR), coarse sand (CS), fine sand (FS), silt (SI), and clay (CL) measured for the same 70 core samples. The data set also includes 1,376 observations of initial moisture content (θ_i) before the 2000 injection experiment started.

[38] The vertical spatial structure of the pedotransfer variables and the spatial correlation between θ_i and each pedotransfer variable is described using vertical variograms and cross-variograms. The layering structure at the site is captured in the vertical variograms and cross-variograms, indicating that these measurements carry significant information about media heterogeneity. Spatial correlation between θ_i and each PTF variable is evident in the vertical cross-variograms. Using the variograms and cross-variograms, heterogeneous fields of the pedotransfer variables are generated using cokriging, in which θ_i is used as the secondary variable. The imperfectly stratified layering structure is captured well in the cokriged fields of the pedotransfer variables. Statistics (mean, minimum, and maximum) for the cokriged estimates compare well with those for the measurements; the vertical spatial variability of the measured data is reproduced well in the cokriged fields.

[39] A site-specific Artificial Neural Network (ANN)-based PTF is developed and a Bayesian method is used to prevent overparameterization. The ANN uses the cokriged heterogeneous fields of pedotransfer variables as input to generated heterogeneous fields of the soil hydraulic parameters. An imperfectly stratified layering structure is present in the ANN-generated fields. While the mean estimates for the soil hydraulic parameters are close to those for measured parameters, ranges of the ANN-generated values are smaller mainly due to smoothed cokriging results, noisy data, and limitations of the ANN models in predicting the soil hydraulic parameters.

[40] It should be noted that, rather than using ANN, we also attempted estimating soil hydraulic parameters directly using θ_i as the secondary variable during cokriging. However, this resulted in negative values for several van Genuchten parameters. We attributed this to the nonlinear relationship between moisture content and the van Genuchten parameters. The nonlinear relationship cannot be captured by cokriging, which is essentially a linear interpolation technique. Therefore we used the two-step procedure, i.e., estimating PTF variables using θ_i as the secondary variable during cokriging and then using ANN to estimate the hydraulic parameters.

[41] Reliability of the generated three-dimensional fields of soil hydraulic parameters is evaluated by simulating the 2000 field injection experiment at the site. The spatial distribution patterns of the moisture plume at different observation times are reproduced well, as examined visually and by Pearson's linear correlation coefficient. Based on computed RMSE and correlation coefficient, a relatively good agreement is observed for simulated and observed moisture content spatial variation at different borehole sites. Unlike our earlier work which used an equivalent homogeneous medium approach to model the heterogeneous media and thus essentially modeled the mean ensemble behavior, this work was able to model the highly variable nature of the observed moisture plume and its splitting within the coarse-textured layer that is sandwiched between two fine-textured layers. The simulated downward movement of the injected water is slightly faster and has a smaller spatial spreading than that observed. This indicates that moisture retention in the z direction is underestimated. Nonetheless, the comparison shows a relatively good agreement for the moisture plume centers and the spatial spreading in the x and y directions. Overall, the heterogeneous soil hydraulic parameter estimates yield relatively good simulation results for the 2000 injection experiment, although site measurements used to determine initial and boundary conditions are sparse.

[42] Our new method of generating heterogeneous soil hydraulic parameters has significant potential implications. The proposed method is generic and can be extended to include other site measurements of varying types through cokriging. For example, if more measurements of pedotransfer variables are available, they can be incorporated in the cokriging to generate more realistic fields. If the dense initial moisture content data set is not available at other sites, other easily obtained geophysical measurements [for example, electrical resistance tomography, *Yeh et al.*, 2002; *Liu and Yeh*, 2004, and ground-penetrating radar, *Kowalsky*

et al., 2005] may be used as the secondary variable for cokriging. Although it requires fitting variogram models and training ANN, the proposed method is a forward one, since, different from traditional inverse methods, it does not solve the Richards' equation iteratively. Nonetheless, our simulation results, with a much less computational burden, are comparable with those obtained from traditional inverse modeling [e.g., *Zhang et al.*, 2004; *Kowalsky et al.*, 2005; *Ward et al.*, 2006].

[43] Uncertainty analysis may be needed in future to facilitate science-based decision making and help focus limited resources on site characterization and remediation. One source of uncertainty is cokriging estimation uncertainty reflected in cokriging variance. On the other hand, parametric uncertainty due to parameter spatial variability has not been explored. The ANN uses a bootstrap method to estimate uncertainty of the estimated ANN coefficients. In future, uncertainty analysis will be conducted to estimate uncertainty bounds for simulated variables of interest. It would also be useful to extend the cokriging and ANN methods to incorporate measurement error.

[44] **Acknowledgments.** The injection site experiments in the year 2000 were conducted as part of the Vadose Zone Transport Field Study at the Hanford Site; Glendon Gee of Pacific Northwest National Laboratory (PNNL) was the project manager. J. Buck Sisson (formerly of Rockwell Hanford Operations, Richland, WA) originally designed the injection test site layout and conducted the first experiments at the site in 1980. The authors are thankful to Jim Yeh and Shlomo Neuman for their thoughtful and constructive review. We are grateful for the useful and constructive comments of the Associate Editor and three anonymous reviewers. The work reported was performed for the CH2M Hill Hanford Group Inc. and the U.S. Department of Energy Office of River Protection under Contract DE-AC06-99RL14047. The first and fourth authors are also supported by the DOE EPSCoR program under contract DE-FG02-06ER46265. The first author conducted this work when he was employed in the Desert Research Institute (DRI). The third author is also supported by NSF-EAR grant 044024. Reference herein to any specific commercial product, process, or service by trade name, trademark, manufacturer, or otherwise, does not necessarily constitute or imply its endorsement, recommendation, or favoring by the United States Government or any agency thereof or its contractors or subcontractors. The views and opinions of the authors do not necessarily state or reflect those of the United States Government or any agency thereof.

References

Aris, R. (1956), On the dispersion of a solute in a fluid flowing through a tube, *Proc. R. Soc. London, Ser. A*, *235*, 67–78.

Cassiani, G., and A. Binley (2005), Modeling unsaturated flow in a layered formation under quasi-steady state conditions using geophysical data constraints, *Adv. Water Resour.*, *28*, 467–477.

Cressie, N. (1991), Statistics of Spatial Data, John Wiley, Hoboken, N. J.

Cole, C. R., M. P. Bergeron, S. K. Wurstner, P. D. Thorne, S. Orr, and M. I. McKinley (2001), Transient Inverse Calibration of Hanford Site-Wide Groundwater Model to Hanford Operational Impacts—1943 to 1996, PNNL-13447, Pacific Northwest National Laboratory, Richland, WA.

Demuth, H., and M. Beale (1992), Neural Network Toolbox Manual, MathWorks Inc., Natick, Massachussetts.

Deutsch, C. V., and A. G. Journel (1998), GSLIB-Geostatistical Software Library and User's Guide, Oxford Univ. Press, New York.

Efron, B., and R. J. Tibshirani (1993), An Introduction to the Bootstrap, Monographs on Statistics and Applied Probability, CRC Press, Boca Raton, Fla.

Fayer, M. J., R. E. Lewis, R. E. Engelman, A. L. Pearson, C. J. Murray, J. L. Smoot, R. R. Randall, W. H. Wegener, and A. H. Lu (1995), Re-Evaluation of a Subsurface Injection Experiment for Testing Flow and Transport Models, PNL-10860, Pacific Northwest National Laboratory, Richland, WA.

Gardner, W. R. (1958), Some steady state solutions of unsaturated moisture flow equations with applications to evaporation from a water table, *Soil Sci.*, *85*, 228–232.

Gee, G. W., and A. L. Ward (2001), Vadose Zone Transport Field Study: Status Report, PNNL-13679, Pacific Northwest National Laboratory, Richland, WA.

Haykin, S. (1994), Neural Networks, A Comprehensive Foundation, 1st ed. Macmillan, New York.

Hecht-Nielsen, R. (1990), Neurocomputing, Addison-Wesley, Boston, Mass.

Hughson, D. L., and T.-C. J. Yeh (2000), An iterative model for three-dimensional flow in variably saturated porous media, *Water Resour. Res.*, *36*(4), 829–840.

Isaaks, E. H., and R. M. Srivastava (1989), An Introduction to Applied Geostatistics, Oxford Univ. Press, New York.

Journel, A. G., and Ch. J. Huijbregts (1978), *Mining Geostatistics*, Elsevier, New York.

Khaleel, R., and E. J. Freeman (1995), Variability and Scaling of Hydraulic Properties for 200 Area soils, Hanford Site WHC-EP-0883, Westinghouse Hanford Company, Richland, WA.

Khaleel, R., J. F. Relyea, and J. L. Conca (1995), Evaluation of van Genuchten-Mualem relationships to estimate unsaturated hydraulic conductivity at low water contents, *Water Resour. Res.*, *31*(11), 2659–2668.

Kowalsky, M. B., S. Finsterle, J. Peterson, S. Hubbard, Y. Rubin, E. Majer, A. Ward, and G. Gee (2005), Estimation of field-scale soil hydraulic and dielectric parameters through joint inversion of GPR and hydrological data, *Water Resour. Res.*, *41*, W11425, doi:10.1029/2005WR004237.

Last, G. V., and T. G. Caldwell (2001), Core Sampling in Support of the Vadose Zone Transport Field Study, PNNL-13454, Pacific Northwest National Laboratory, Richland, WA.

Last, G. V., T. G. Caldwell, and A. T. Owen (2001), Sampling of Boreholes WL-3A through 12 in Support of the Vadose Zone Transport Field Study, PNNL-13631, Pacific Northwest National Laboratory, Richland, WA.

Li, B., and T.-C. J. Yeh (1999), Cokriging estimation of the conductivity field under variably saturated flow conditions, *Water Resour. Res.*, *35*(12), 3663–3674.

Liu, S.-Y., and T.-C. J. Yeh (2004), An integrative approach for monitoring water movement in the vadose zone, *Vadose Zone J.*, *3*(2), 681–692.

MacKay, D. J. C. (1992), Bayesian interpolation, *Neural Comput.*, *4*(2), 415–447.

Mayes, M. A., P. M. Jardine, T. L. Mehlhorn, B. N. Bjornstad, J. L. Ladd, and J. M. Zachara (2003), Transport of multiple tracers in variably saturated humid region structured soils and semi-arid region laminated sediments, *J. Hydrol.*, *275*, 141–161.

Meyer, P. D., M. L. Rockhold, and G. W. Gee (1997), Uncertainty Analysis of Infiltration and Subsurface Flow and Transport for SDMP Sites, NUREG/CR-6565, PNNL-11705, U.S. Nuclear Regulatory Commission, Office of Nuclear Regulatory Research, Washington, DC.

Minasny, B., A. B. McBratney, and K. L. Bristow (1999), Comparison of different approaches to the development of pedotransfer functions for water-retention curves, *Geoderma*, *93*, 225–253.

Pace, M. N., M. A. Mayes, P. M. Jardine, T. L. Mehlhorn, J. M. Zachara, and B. N. Bjornstad (2003), Quantifying the effects of small-scale heterogeneities on flow and transport in undisturbed cores from the Hanford formation, *Vadose Zone J.*, *2*, 664–676.

Pachepsky, Y. A., D Timlin, and G. Varallyay (1996), Artificial neural networks to estimate soil water retention from easily measurable data, *Soil Sci. Soc. Am. J.*, *60*, 727–733.

Pachepsky, Y. A., D. Timlin, and L. Ahuja (1999), Estimating saturated soil hydraulic conductivity using water retention data and neural networks, *Soil Sci.*, *164*, 552–560.

Pyrcz, M. J., and C. V. Deutsch (2003), The whole story on the hole effect, edited by S. Searston, Geostatistical Association of Australasia, Newsletter 18.

Rockhold, M. L., R. E. Rossi, and R. G. Hills (1996), Application of similar media scaling and conditional simulation for modeling water flow and tritium transport at the Las Cruces Trench Site, *Water Resour. Res.*, *32*(3), 595–609.

Rockhold, M. L., C. J. Murray, and M. J. Fayer (1999), Conditional simulation and upscaling of soil hydraulic properties, in *Characterization and Measurement of the Hydraulic Properties of Unsaturated Porous Media*, edited by M. Th. van Genuchten, F. J. Leij, and L. Wu, p. 1391-1401, Univ. of Calif. Press, Berkeley.

Schaap, M. G., and W. Bouten (1996), Modeling water retention curves of sandy soils using neural networks, *Water Resour. Res.*, *32*, 3033–3040.

Schaap, M. G., F. J. Leij, and M. Th. van Genuchten (1998), Neural network analysis for hierarchical prediction of soil hydraulic properties, *Soil Sci. Soc. Am. J.*, *62*, 847–855.

Schaap, M. G., F. J. Leij, and M. Th. van Genuchten (2001), Rosetta: a computer program for estimating soil hydraulic parameters with hierarchical pedotransfer functions, *J. Hydrol.*, *251*, 163–176.

Schaap, M. G., P. J. Shouse, and P. D. Meyer (2003), Laboratory Measurements of the Unsaturated Hydraulic Properties at the Vadose Zone Transport Field Study Site, PNNL-14284, Pacific Northwest National Laboratory, Richland, Washington.

Sisson, J. B., and A. H. Lu (1984), Field Calibration of Computer Models for Application to Buried Liquid Discharges: A Status Report, RHO-ST-46P, Rockwell Hanford Operations, Richland, WA.

Srivastava, R., and T.-C. J. Yeh (1992), A three-dimensional numerical model for water flow and transport of chemically reactive solute through porous media under variably saturated conditions, *Adv. Water Resour.*, *15*, 275–287.

van Genuchten, M. Th. (1980), A closed-form equation for predicting the hydraulic conductivity of unsaturated soils, *Soil Sci. Soc. Am. J.*, *44*, 892–898.

Wang, W., S. P. Neuman, T. Yao, and P. J. Wierenga (2003), Simulation of large-scale field infiltration experiments using a hierarchy of models based on public, generic, and site data, *Vadose Zone J.*, *2*, 297–312.

Ward, A. L., T. G. Caldwell, and G. W. Gee (2000), Vadose Zone Transport Field Study: Soil Water Content Distributions by Neutron Moderation, PNNL-13795, Pacific Northwest National Laboratory, Richland, WA.

Ward, A. L., Z. F. Zhang, and G. W. Gee (2006), Upscaling unsaturated hydraulic parameters for flow through heterogeneous, anisotropic sediments, *Adv. Water Resour.*, *29*(2), 268–280.

Yates, S. R., and A. W. Warrick (1987), Estimating soil water content using cokriging, *Soil Sci. Soc. Am. J.*, *51*, 23–30.

Ye, M., R. Khaleel, and T.-C. J. Yeh (2005), Stochastic analysis of moisture plume dynamics of a field injection experiment, *Water Resour. Res.*, *41*, W03013, doi:10.1029/2004WR003735.

Yeh, T.-C. J., and S. Liu (2000), Hydraulic tomography: Development of a new aquifer test method, *Water Resour. Res.*, *36*(8), 2095–2105.

Yeh, T.-C. J., and J. Zhang (1996), A geostatistical inverse method for variably saturated flow in the vadose zone, *Water Resour. Res.*, *32*(9), 2757–2766.

Yeh, T.-C. J., L. W. Gelhar, and A. L. Gutjahr (1985a), Stochastic analysis of unsaturated flow in heterogeneous soils: 1. Statistically isotropic media, *Water Resour. Res.*, *21*(4), 447–456.

Yeh, T.-C. J., L. W. Gelhar, and A. L. Gutjahr (1985b), Stochastic analysis of unsaturated flow in heterogeneous soils: 2. Statistically anisotropic media, *Water Resour. Res.*, *21*(4), 457–464.

Yeh, T.-C. J., L. W. Gelhar, and A. L. Gutjahr (1985c), Stochastic analysis of unsaturated flow in heterogeneous soils: 3. Observations and applications, *Water Resour. Res.*, *21*(4), 465–471.

Yeh, T.-C. J., S. Liu, R. J. Glass, K. Baker, J. R. Brainard, D. L. Alumbaugh, and D. LaBrecque (2002), A geostatistically based inverse model for electrical resistivity surveys and its applications to vadose zone hydrology, *Water Resour. Res.*, *38*(12), 1278, doi:10.1029/2001WR001204.

Yeh, T.-C. J., M. Ye, and R. Khaleel (2005), Estimation of effective unsaturated hydraulic conductivity tensor using spatial moments of observed moisture plume, *Water Resour. Res.*, *41*, W03014, doi:10.1029/2004WR003736.

Zhang, J., and T.-C. J. Yeh (1997), An iterative geostatistical inverse method for steady flow in the vadose zone, *Water Resour. Res.*, *33*(1), 63–71.

Zhang, Z. F., A. L. Ward, and G. W. Gee (2004), A combined parameter scaling and inverse technique to upscale the unsaturated hydraulic parameters for heterogeneous soils, *Water Resour. Res.*, *40*, W08306, doi:10.1029/2003WR002925.

R. Khaleel, Fluor Government Group, P. O. Box 1050, Richland, WA 99352, USA.

M. G. Schaap, Department of Environmental Sciences, University of California, Riverside, CA 92507, USA.

M. Ye, School of Computational Science and Department of Geological Sciences, Florida State University, Tallahassee, FL 32306, USA. (mingye@scs.fsu.edu)

J. Zhu, Division of Hydrologic Sciences, Desert Research Institute, Nevada System of Higher Education, Las Vegas, NV 89119, USA.